Scientia Horticulturae 277 (2021) 109840

Contents lists available at ScienceDirect

Scientia Horticulturae

journal homepage: www.elsevier.com/locate/scihorti

Use of X-ray computed tomography and 3D image analysis to characterize internal browning in 'Fuji' apples after exposure to CO_2 stress

Kenias Chigwaya [a,d], Anton du Plessis [b,c], Daniël W. Viljoen [d], Ian J. Crouch [d], Elke M. Crouch [a,*]

[a] Department of Horticultural Science, Faculty of AgriSciences, Stellenbosch University, South Africa
[b] Stellenbosch University CT Facility, Stellenbosch University, South Africa
[c] Physics Department, Faculty of Science, Stellenbosch University, South Africa
[d] ExperiCo (Agri-Research Solutions), Idas Valley, Stellenbosch, 7609, South Africa

ARTICLE INFO

Keywords:
High-resolution scans
Internal browning
Low-resolution scans
Malus domestica Borkh
Porosity
X-ray computed tomography

ABSTRACT

In this study X-ray computed tomography (X-ray CT) was used to determine microstructural properties of 'Fuji' apple *(Malus domestica* Borkh.*)* tissue affected by internal browning (IB) and unaffected tissue after short-term exposure (3 days) to a storage atmosphere with 0.1 % O_2 and 50 % CO_2. The incidence of IB disorders were concentrated in the core of the fruit. IB developed in 31 % of fruit at varying degrees of severity, due to differences in microstructural and morphological properties of individual fruit. X-ray CT scanning was able to give pore and cell microstructural information such as porosity, length, sphericity, connectivity, equivalent diameter, and anisotropy. High-resolution scans showed that fruit tissue with IB had a lower total porosity and pore connectivity compared to unaffected fruit tissue, possibly due to membrane damage and flooding of intercellular spaces with cellular fluids. The pores in affected brown tissue were significantly more spherical as compared to the other tissue types. Low-resolution (full fruit) scans showed that the density of fruit tissue affected by IB was not significantly different from that of unaffected fruit tissue. Low porosity in the fruit core region restricts gas transport and predisposes the core region to CO_2 induced IB. This work provided a novel and in-depth insight into the effects of short-term high CO_2/low O_2 stress conditions on the microstructural properties of South African grown 'Fuji' apples. Furthermore, this study showed that tissue microstructure influences the susceptibility of different regions within the same fruit to stress-induced IB symptoms.

1. Introduction

Fuji is an economically important apple cultivar globally and has maintained a significant global apple production share in previous years (Ferree and Warrington, 2003). In South Africa, Fuji is the 6th most cultivated apple cultivar occupying 2388 of the 24970 ha under apple production (HORTGRO, 2019). In addition, 'Fuji' apples constituted 3, 014,535 of the 33,871,534 apple cartons exported from South Africa in 2019 (HORTGRO, 2019). Long-term storage of 'Fuji' apples has been made possible through the use of controlled atmosphere (CA) and delayed CA storage techniques (Argenta et al., 2000; Tanaka et al., 2018). CA storage utilises an elevated CO_2 and reduced O_2 concentration to lower respiration rate and this extends the storage life of fruit (Pedreschi et al., 2009a). Although CA storage has the capacity to maintain quality during long-term storage, it can also result in the incidence of storage disorders such as internal browning (IB) especially when CO_2 levels are elevated (Lau, 1998; Elgar et al., 1999). To mimic IB types such as CO_2 damage which occur during long-term CA storage, 'Fuji' apples are sometimes stored at high CO_2 and low O_2 levels for short durations. Short-term exposure of 'Fuji' apples to such conditions has been used as an accurate predictor of fruit susceptibility to CA-induced IB (Argenta et al., 2002). IB is characterised by patches of brown flesh, with or without cavities that develop in the apple tissue (Argenta et al., 2002).

Due to diffusion limitations, reduced O_2 and elevated CO_2 levels within the storage atmosphere can result in the establishment of a concentration gradient within the apple tissue which causes a decrease of the O_2 partial pressure and an increase of CO_2 partial pressure towards the core of the fruit (Ho et al., 2013). This can result in a change of the fruit metabolic pathway from the normal respiration to fermentation (Saquet et al., 2003; Mellidou et al., 2014). Metabolomics and proteomic studies have confirmed the impairment of the oxidative pathway and a

* Corresponding author.
E-mail address: elke@sun.ac.za (E.M. Crouch).

https://doi.org/10.1016/j.scienta.2020.109840
Received 27 March 2020; Received in revised form 29 September 2020; Accepted 30 October 2020
Available online 5 November 2020

shift to the fermentation pathway when fruit is stored under extreme CA (Pedreschi et al., 2008, 2009a, 2009b). The shift to the fermentation pathway will result in less available energy to maintain membrane integrity and this causes membrane damage by reactive oxygen species leading to loss of compartmentalisation and browning (Mellidou et al., 2014). Responses of 'Fuji' apples after short-term exposure to elevated CO_2 levels have been investigated by Argenta et al. (2002). They found that the severity of the CO_2 damage was higher in fruit exposed to 20 kPa CO_2 after harvest than in fruit exposed to 20 kPa CO_2 after 8 months of CA storage. Ke et al. (1990) found that 'Bartlett' pears exposed to 50 % CO_2 had a higher incidence of browning disorders compared to those exposed to 80 % CO_2.

To fully understand events happening at the microstructural level as a result of IB incidence, it is necessary to evaluate the fruit microstructure quantitatively and qualitatively. Traditionally, light and confocal microscopy have been used to evaluate fruit microstructure (Schotsmans et al., 2004; Pieczywek and Zdunek, 2012). However, these methods are limited in their penetration depth and reliance on destructive analysis of thin 2D sections to estimate volumetric measurements of 3D structures (Herremans et al., 2013), potentially missing important information. A method for isolating and measuring the shape and size of apple cells from 2D images was proposed by McAtee et al. (2009), however, this method still provides limited 3D geometric information. X-ray computed tomography (Xray CT) is an innovative imaging technique that can be utilised in the acquisition of 3D spatial data from intact fruit samples (Ting et al., 2013). X-ray CT has been gaining popularity due to its non-destructive nature and ability to image 3D structures. It has a high penetration depth and does not require tedious sample preparation as some other methods (Vicent et al., 2017). The use of X-ray CT in apple fruit microstructure evaluations has been explored by different researchers. Ting et al. (2013) used this technique to evaluate microstructural properties of different apple cultivars while Herremans et al. (2013) used it in the characterisation of 'Braeburn' browning disorder, which occurs during CA storage of 'Braeburn' apples. Diels et al. (2017) explored its use in the assessment of bruising in apples, bruising occurs during post-harvest handling and is characterised by flattening and discolouration of the tissue. More recently, Poles et al. (2020) used X-ray CT to investigate the interactions between cell morphology and texture-juiciness properties of fourteen apple cultivars, which included 'Fuji'. Their study showed that 'Fuji' apples had the highest fraction of small pores, this property may increase the susceptibility of 'Fuji' to IB symptoms during CA storage since small pores are limited in their gas transport capacity.

The objective of this present study was to compare microstructural properties of fruit tissue affected by CO_2 induced IB with unaffected fruit tissue by using X-ray CT and 3D image analysis techniques. This gave an in-depth insight into the differences in microstructure between 'Fuji' fruit tissue that developed IB and unaffected fruit tissue.

2. Materials and methods

2.1. Fruit material

'Fuji' apples (*Malus domestica* Borkh.) were harvested in March 2018 from Wakkerstroom farm located in the Koue Bokkeveld area in the Western Cape Province, South Africa. The fruit were harvested at shoulder height from each tree, from either side of the canopy. Fruit were harvested into lug boxes and were transported to the fruit evaluation laboratory at the Department of Horticultural Sciences, Stellenbosch University, South Africa. Maturity indexing was done on arrival at the lab to determine the maturity status of the fruit at harvest.

2.2. Fruit quality evaluations at harvest

To determine fruit maturity at harvest, fruit were evaluated for diameter, mass, height, ground peel colour, blush percentage, flesh firmness, titratable acidity (TA), total soluble solutes (TSS) and starch breakdown. TA and TSS were measured on a pooled sample of 20 fruit whereas the other parameters were determined on each of 40 fruit. Fruit diameter, mass and height were measured using a Cranston gauge and electronic balance, both fitted to the fruit texture analyser (FTA 2007, Guss, Strand, South Africa). Ground peel colour of fruit was rated from 0.5 (green) to 5 (yellow), using the South African Industry colour chart for apples and pears (Unifruco Research Services, Bellville, South Africa). The blush percentage was determined by trained reviewers who estimated the percentage of the fruit surface covered by a red blush (0 % for no red blush and 100 % for full red blush). Fruit firmness was measured equatorially on opposite sides of the fruit on a peeled surface using a universal fruit texture analyser, fitted with a 7.9 mm diameter probe. Titratable acidity was measured by titration of fruit juice using an automated titrator (Metrohm AG 760. Harison, Switzerland). Total soluble solutes content was measured on a drop of expressed fruit juice using a hand-held digital refractometer (Atago Digital-Refractometer PR-32, Tokyo, Japan). Percentage starch conversion was estimated using the iodine test with a starch conversion chart (Unifruco Research Services, Bellville, South Africa) with a scale of 0 % to 100 %, where 0 % was totally stained and 100 % was totally unstained.

2.3. High CO_2 /low O_2 stress treatment

After harvesting, 400 fruit were subjected to a storage atmosphere with 0.1 % O_2 and 50 % CO_2 for 3 days at room temperature (21 °C). This was done by placing the fruit in a tightly closed controlled atmosphere bin and then pumping in CO_2 until the controlled atmosphere bin comprised of 50 % CO_2. The level of O_2 in the controlled atmosphere bin after CO_2 enrichment was 0.1 %. The level of gases inside the controlled atmosphere bin was measured using a handheld gas analyser (ICA 350 Dual Analyser, Storage Control Systems, Inc. UK). The level of CO_2 inside the bin was maintained at 50 % throughout the duration of the experiment. At the end of the 3 days, all the fruit were taken out of the bin and each of the fruit were cut to evaluate the incidence of IB.

2.4. Intensity of browning incidence

To quantify the IB incidence, the intensity index chart in Fig. 1 was used after each of the fruit was cut into two halves at the equator. An intensity index of 0 was used if the core of the apple did not have any IB incidence. An intensity index of 1 was used if up to 20 % of the apple core was affected by IB. An intensity index of 2 was used if up to 40 % of the apple core was affected by IB. If 60 % of the apple core was affected by IB, an intensity index of 3 was given to such fruit. Fruit in which the core was between 60 and 80 % affected by IB was given an index of 4. In severe cases were the entire fruit core was affected by IB, an intensity index of 5 was given. After evaluation and scoring of fruit, 20 fruit with IB and 20 fruit without IB were randomly selected for low-resolution and high-resolution X-ray CT scanning. In low-resolution whole fruit scans, the two cut halves had to be carefully placed back on top of each other and secured with a cling wrap before scanning took place.

2.5. Low-resolution X-ray CT (whole fruit scans)

To determine grey values and tissue density, low-resolution X-ray CT scanning was done on 40 whole apples at the Stellenbosch University Central Analytical Facility. Twenty of the fruit had core IB while 20 did not have core IB. The General Electric V|Tome|X L240 X-ray CT scanner manufactured by General Electric Sensing and Inspection Technologies/ Phoenix X-ray (Wunstorf, Germany) contains two X-ray tubes, one with a reflection-type target and the other with a transmission target (du Plessis et al., 2016). The average time per scan was 30 min and 2300 projection images were captured. The samples were scanned at a voltage of 100 kV and a current of 100 μA, these parameters were able to give a voxel size of 60 μm. A series of 2D X-ray projection images were

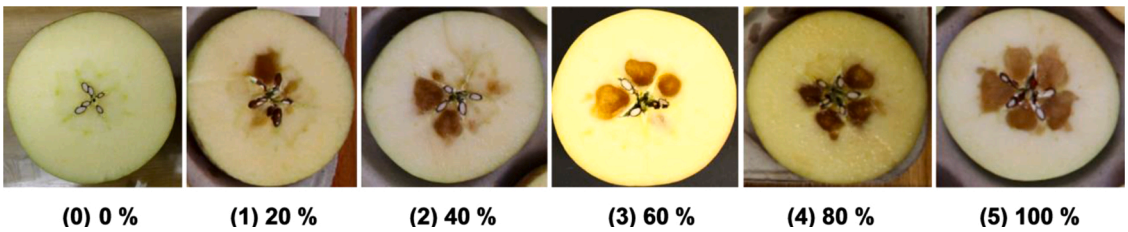

Fig. 1. Reference used for internal browning (IB) intensity index. Fruit with a score of 0 did not show any IB in the core while fruit with an intensity index of 5 had a 100 % IB coverage of the core region.

obtained, and these were reconstructed using reconstruction software Datos|x®2.1 (General Electric Sensing & Inspection Technologies GmbH, Phoenix, Wunstorf, Germany) to generate virtual 3D volumes.

2.6. High-resolution X-ray CT

Cylindrical samples for high-resolution X-ray CT were obtained using a cork borer of 5 mm diameter. Each sample had a diameter of 5 mm and was 15 mm long. For apples with core browning, 2 samples were scanned, one from the brown region and another from a white region without browning (Fig. 2). For apples without any form of browning, one sample was taken from the apple core. The samples from the non-brown apples acted as the control samples. In total, 60 samples were scanned at high-resolution, 20 brown samples from fruit with IB, 20 white samples from fruit with IB and 20 white samples from unaffected fruit. The cylindrical tissue samples were cut on either end to about 15 mm length and wrapped in parafilm to avoid dehydration during scanning. The samples were then loaded individually onto the Nanotom S instrument (General Electric Sensing and Inspection Technologies/ Phoenix X-ray, Wunstorf, Germany) at the Stellenbosch University Central Analytical Facility for scanning. Various system settings were tested to optimize the scan quality. A series of 2600 projection images were obtained as the sample was rotated 360°. The samples were scanned at a voltage of 60 kV and a current of 240 μA giving a voxel size of 3 μm. The average scan time was 45 min per sample. A series of 2D X-ray projection images were obtained, and these were reconstructed into 3D volumes using reconstruction software Datos|x®2.1 (General Electric Sensing & Inspection Technologies GmbH, Phoenix, Wunstorf, Germany) to generate virtual 3D images.

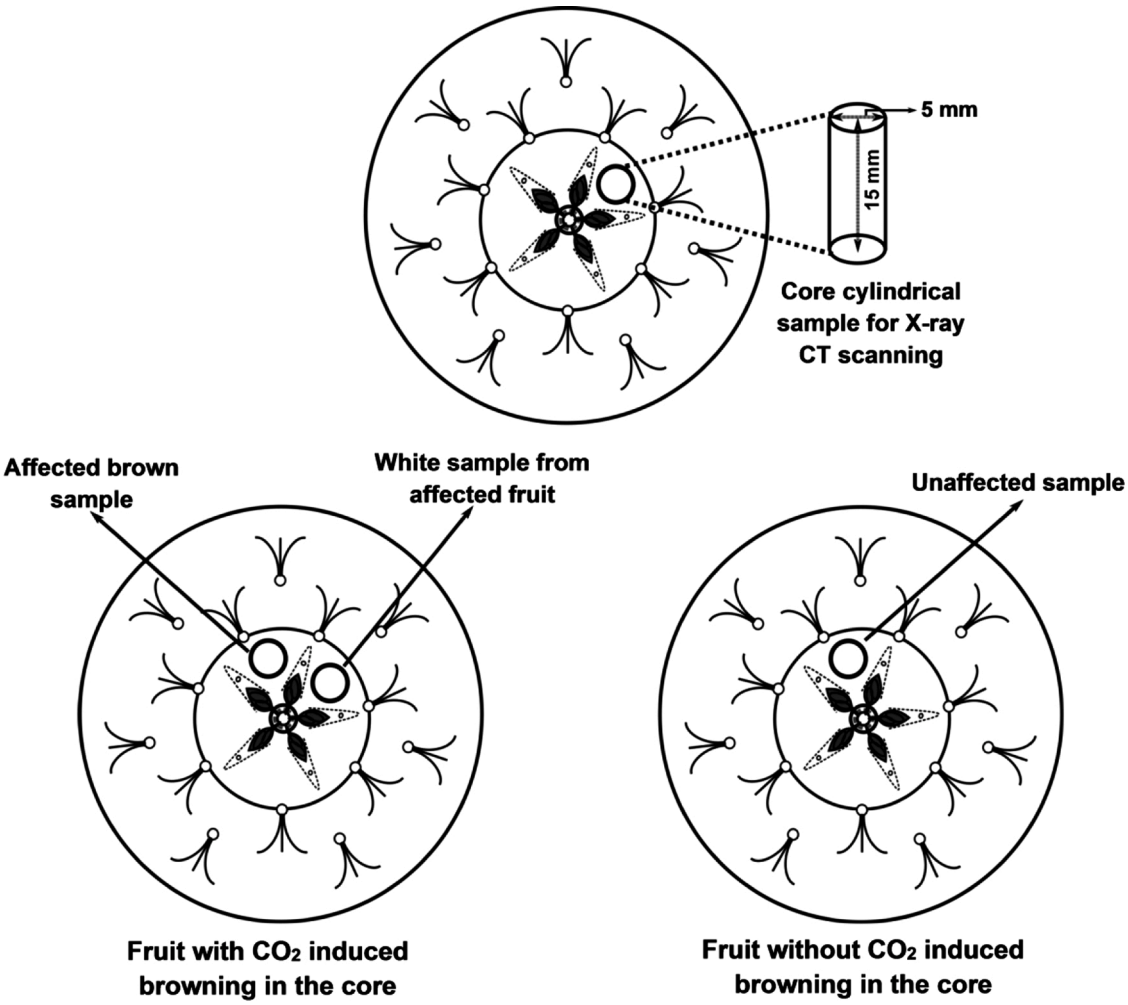

Fig. 2. Schematic presentation for the sampling positions from fruit with CO_2 induced browning in the core and fruit without CO_2 induced browning.

2.7. Image analysis

To extract suitable quantitative information from X-ray CT images, it is necessary to perform 3D image analysis. Image analysis was done on 3D volumes generated after reconstruction. The polychromacity of the X-ray beam gives rise to the beam hardening effect (du Plessis et al., 2020). As a result, beam hardening correction of level 2 (software specific value) had to be applied to correct this artefact. The beam hardening effect causes the appearance of artefacts, i.e., continuous variation in grey values within the reconstructed volume depending on the variation of object thickness at different positions (Boas and Fleischmann, 2012). Analysing the whole image in its entirety can be an arduous and time-consuming exercise, hence it was necessary to select a region of interest (ROI) from the original image (Schoeman et al., 2016). Although a ROI is smaller in size compared to the original image, it was important to ensure that the selected ROI was large enough to be statistically representative of the whole sample. In this study a ROI cube measuring $2.5 \times 2.5 \times 2.5$ mm was used. This volume of 15.625 mm^3 was larger than the lower limit for a representative volume element of 1.3 mm^3 that was proposed by Mendoza et al. (2007).

After this, it was necessary to remove random noise that occurs during scanning. Filtering was done using a median filter for cell analysis in Avizo 2019.1 (VSG, Bordeaux, France) and an adaptive gauss filter for pore analysis in VGStudio Max 3.2 (Volume Graphics GmbH, Heidelberg, Germany). After filtering, the image was segmented into the constituent cells and pores so that subsequent analysis procedures could be carried out. Automatic thresholding using Otsu's method was done to create a binary image consisting of only cells and pores (Otsu, 1979). Otsu's thresholding involves the defining of a single grey value to separate regions of the image based on analysis of the image histogram (Otsu, 1979; Iassonov et al., 2009; Zhang et al., 2017). Voxels containing grey values lower than this threshold value are regarded as background while those with grey values higher than the threshold value are regarded as sample material (Schoeman et al., 2016). Segmentation of X-ray CT images using Otsu method has been used by Herremans et al. (2013) in Braeburn apples, Muziri et al. (2016) in 'Forelle' pears and Ting et al. (2013) in determination of differences in microstructural properties of different apple cultivars. After image thresholding, 3D image analysis was then done, and various microstructural properties determined (Table 1). 3D image analysis was done using Avizo 2019.1 (VSG, Bordeaux, France), CTAn 1.18.0.0 (Bruker microCT, Kontich, Belgium) and VGStudio Max 3.2 (Volume Graphics GmbH, Heidelberg, Germany).

2.8. Cell isolation

Automatic segmentation of individual cells was not possible due to insufficient contrast between cytoplasm and cell wall. Hence, segmentation of individual cells was done using the watershed separation algorithm (Wang et al., 2020). The 3D region that was identified as cells after segmentation needed to be further segmented into individual cells to allow for the quantification of individual cell properties. This was implemented using the "separate objects" module in Avizo 2019.1. The watershed method is a powerful morphological tool for image segmentation. It derives its name from the geographical meaning of watershed, which refers to the ridge that divides areas drained by different river systems (Ruparelia, 2012). If the image is viewed as a landscape, the watershed lines determine boundaries which separates image regions (Ruparelia, 2012).

The algorithm works by calculating the chamfer distance map of the binary image, in which greyscales represent the distance from that pixel to the nearest black (background) pixel, regardless of direction. The chamfer distance map which computes the distance as a discrete approximation produces a mountain peak at the centre of each of the cells. In this study, the "separate objects/chamfer conservative" module in Avizo 2019.1 was used to compute watershed lines on the binary image. All cells that intersected the dataset borders after watershed separation were removed to exclude incomplete individual cells from cell measurements (Fig. 3). After watershed separation, some cells were not fully separated, and such cells had to be excluded from the image since they give rise to inaccurate results. A virtual sieve was used to remove incorrectly segmented cells and unseparated clumps of cells (Fig. 3). Based on literature, all individual objects with a length larger than 400 μm and a sphericity index lower than 0.75 were removed from the 3D model (Herremans et al., 2015; Wang et al., 2020). This allowed the 3D model of the image to comprise of only correctly segmented cells. This protocol was validated by Herremans et al. (2015) by manually segmenting individual cells and they found no significant differences in this method and manually segmented individual cells. Failure of the watershed algorithm to detect cell boundaries in affected tissue samples proved that there was disruption of cellular structure in brown affected tissue (Fig. 4).

Table 1
Morphometric parameters used to describe 3D X-ray CT images, based on Herremans et al. (2013), with modifications.

Microstructural parameter	Unit	Description
Volume	mm^3	Volume of object.
Area	mm^2	Area of the object boundary.
Length	μm	Maximum of the ferret diameters used over a range of angles.
Width	μm	Minimum of the ferret diameters used over a range of angles.
Equivalent diameter	μm	The diameter of a sphere of equivalent volume as the irregularly shaped object.
Anisotropy	–	Measure of preferential alignment of structures. This value is scaled from 0 for total isotropy to 1 for total anisotropy.
Euler number	–	It gives information about the connectivity of a 3D structure. Higher values indicate poorly connected structures and lower values for better connected structures.
Connectivity	–	The number of connections between matrix structures per unit volume, based on Euler number.
Total Porosity	%	Pore volume divided by the total volume.
Closed porosity	%	The connected assemblage of space (black) voxels that is fully surrounded on all sides in 3D by solid (white) voxels.
Open porosity	%	Any space located within a solid object or between solid objects with connection in 3D space with outside space.
Sphericity	–	measures the ratio of the surface area of a sphere with the same volume as the cell/pore to its surface area.

2.9. Calculation of tissue density

To enable calculation of the densities of different tissue regions in the apple tissue, a reference of known density (2.21 gcm^{-3}) was scanned together with the apple during low-resolution (whole fruit) scanning. This made it possible to calculate the density of a given region of interest (ROI) based on the density of the reference using formula 1. The tissue density was determined for white unaffected fruit tissue, white tissue from affected fruit and brown affected fruit tissue. The density calibration was developed and validated by Guelpa et al. (2015) in maize (*Zea mays* L.) kernels.

$$\text{Relative density} = \frac{\text{Mean grey value of ROI}}{\text{Mean grey value of reference}} \times 2.21\ gcm^{-3} \quad (1)$$

2.10. Data analysis

To determine if there were differences amongst the different browning scores, the data was first transformed using logit

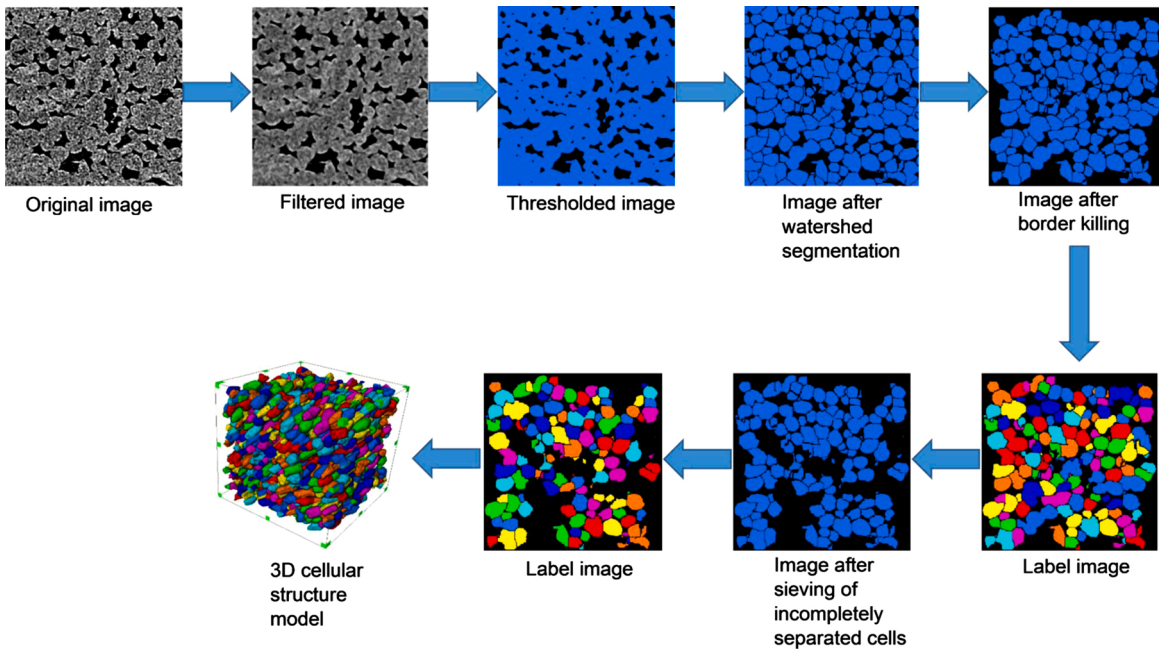

Fig. 3. Schematic representation of the procedure followed for the isolation of individual cells and measurement of individual cell parameters using Avizo 2019.1.

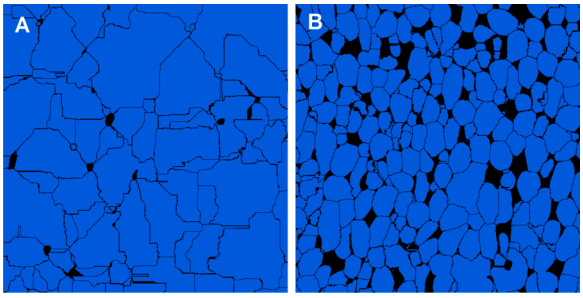

Fig. 4. Thresholded 2D binary images of A – Brown affected core region tissue sample and B – unaffected core region tissue sample after application of the 'separate objects' module in Avizo 2019.1. The separate objects module computes watershed lines to separate n neighbouring cells. The cells are in blue and the pores are in black. Tissue samples were obtained from 'Fuji' apples. The volume of the region of interest was 15.625 mm^3 (2.5 × 2.5 x 2.5 mm) (For interpretation of the references to colour in this figure legend, the reader is referred to the web version of this article).

transformation and ANOVA was done on the transformed data using STATISTICA Version 13.1 (StatSoft Inc., Tulsa, USA). The data was analysed as a completely randomised design (CRD) to compare the differences amongst the different browning scores. Data for pore and cell properties was analysed as a CRD with 11 replicates for affected brown tissue, 15 replicates for white tissue from affected fruit and 17 replicates for unaffected tissue. The data was also analysed using STATISTICA and all mean separations were done using Fisher's LSD test at a significance level of 5 %.

3. Results

3.1. Fruit maturity at harvest

Table 2 presents the maturity parameters of 'Fuji' apples that were used in this study. Maturity at harvest is an important factor that affects the quality and storage potential of apples. The quality and storage potential can be affected by either early harvest or late harvest especially when the fruit are intended for long-term storage. The apples used in this study were harvested during the commercial harvest period in 2018 and the maturity indices show that the apples were at an advanced maturity at the time of harvest.

Table 2
Physiochemical properties (± standard deviation) of 'Fuji' apples used in this study at harvest.

Parameter	Value
Firmness (N)	75.64 ± 5.93
Diameter (mm)	71.65 ± 6.09
Mass (g)	166.13 ± 27.01
Height (mm)	61.86 ± 4.56
TA (%)	0.31 ± 0.02
TSS (%)	13.61 ± 0.77
Ground peel colour (Chart index)	3.31 ± 0.32
Blush percentage (%)	47.55 ± 19.04
Starch breakdown (%) (Chart index)	80.87 ± 19.49

3.2. Browning intensity index

The results in Table 3 show that 69 % of the fruit had an intensity index of 0, meaning that they did not have any IB symptoms. 11 % of the fruit had an intensity index of 1, showing that 20 % of the core was affected by IB. 7 % of the fruit had an intensity index of 2, meaning that up to 40 % of the core was affected by IB. Six percent of the fruit had a browning intensity index of 3, meaning that up to 60 % of the core region was affected by IB. 4 % of the fruit had up to 80 % of their core being affected by IB and 3 % of the fruit had their entire core region affected by IB.

Table 3
Browning intensity index of fruit after the high CO_2/low O_2 stress treatment. Number of apples at each browning intensity index was expressed as a percentage of the total number of fruit.

Browning intensity index	0	1	2	3	4	5
Percentage of total fruit (%)	69 a	11 b	7 bc	6 bc	4 c	3 c
P-value	*< 0.0001*					

3.3. Morphometric parameters of pores

Table 4 represents the 3D morphometric parameters of pores. The number of closed pores was not significantly different amongst the tissue samples. Affected brown samples had a closed porosity of 3.1 % which was significantly lower than the closed porosity of white samples from affected fruit (5.1 %) and unaffected samples (5.9 %). Affected brown samples had an open porosity of 0.9 % which was significantly lower than the open porosity of white samples from affected fruit (6.2 %) and unaffected samples (6.4 %). The total porosity, which is a sum of the open and closed porosity was significantly lower in affected brown samples (4 %) and significantly higher in white samples from affected fruit samples (10.9 %) and unaffected samples (11.9 %) (Fig. 5). The connectivity of the pores was significantly higher in unaffected samples (745.7) and white samples from affected fruit (705.6) compared to affected brown samples which had a connectivity of just 52.2. In terms of length, pores from unaffected samples and white samples from affected fruit were significantly longer with lengths of 120.07 μm and 128.65 μm, respectively. Pores from affected brown samples had a significantly smaller average length of only 95.43 μm. Pores from affected brown tissue had a significantly high sphericity of 0.882 compared to pores in white samples from affected fruit (0.828) and unaffected tissue samples (0.849). Sphericity is the measure of how closely the shape of an object approaches that of a mathematically perfect sphere. Pore anisotropy was significantly lower in affected brown tissue (0.765) as compared to white tissue samples from affected fruit (0.811) and unaffected tissue samples (0.792). Anisotropy refers to the existence of a preferential alignment of the pores and is calculated by performing a mean intercept length analysis. Most pores in all tissue types had an equivalent diameter of less than 160 μm (Fig. 6). In general, for all the pore parameters evaluated the white tissue samples (white tissue from affected fruit and unaffected tissue) did not differ significantly but differed significantly from the brown tissue samples. Pore parameters such as porosity, pore connectivity, number of closed pores and pore length were significantly higher in the white samples compared to the brown samples (Table 4).

3.4. Morphometric parameters of cells

Table 5 represents the 3D morphometric parameters of cells. The length and thickness of the cells did not differ significantly amongst the different tissue samples. There was a significant difference amongst the different tissue types in terms of the width of the cells. Cells from brown affected core tissue samples had the largest width (174.32 μm) as compared to cells from white unaffected core tissue samples (162.74 μm) and white tissue samples from affected fruit (160.86 μm). The surface area of the cells from the different tissue samples also differed significantly. Cells from brown affected tissue samples had the largest surface area (0.155 mm^2) as compared to cells from unaffected tissue samples (0.139 mm^2) and white tissue samples from affected fruit (0.139 mm^2). There was a significant difference amongst the different tissue types in terms of the euler connectivity of the cells. Cells from brown affected tissue samples had the lowest euler3D (0.637) compared to cells from white unaffected tissue samples (0.921) and white tissue samples from affected fruit (0.902). Euler number indicates the connectedness of 3D structures; higher values indicate poorly connected structures while lower values indicate highly connected structures. The different tissue types did not differ significantly in terms of anisotropy and EqDiameter. The sphericity of cells in brown affected tissue samples was significantly lower (0.688) as compared to the sphericity of cells in white tissue samples from affected fruit (0.767) and unaffected tissue samples (0.773). Due to disruption of cellular structure, cell boundaries in affected brown samples were destroyed and could not be detected by the watershed algorithm (Fig. 4). This resulted in only a few cells being able to be properly segmented for cell analysis.

3.5. Tissue density

Fruit were scanned at low-resolution with a reference of known density and this made it possible to calculate the densities of the different regions of interest within the fruit tissue based on the measured grey values of the fruit tissue and known density of the reference. The density of fruit tissue affected by IB (1.278 ± 0.0046 g/cm^3) did not differ significantly from that of unaffected tissue (1.268 ± 0.0059 g/cm^3). The only differences were seen in the contrasting greyscale intensities between fruit tissue affected by IB and fruit tissue without IB. Fruit tissue with IB was characterised by a light grey colour (Fig. 7).

4. Discussion

'Fuji' apples sometimes develop flesh browning disorders during CA storage (Argenta et al., 2000; Tanaka et al., 2018). In addition to fungal decay and superficial scald, CO_2 induced IB has been identified as one of the major causes of 'Fuji' apple losses during storage (Argenta et al., 2020). The elevated CO_2 concentration during CA storage can induce the incidence of IB in cultivars such as 'Pink Lady' and 'Fuji' (de Castro et al., 2007; Argenta et al., 2020). CO_2 induced IB in apples is a result of oxidative damage which occurs as a result of high CO_2 concentration coupled with low O_2 levels in the storage atmosphere (Lau, 1998; Argenta et al., 2000).

CO_2 damage is reduced by the use of antioxidants such as diphenylamine (DPA) and this shows that the disorder is clearly a result of oxidative stress (Argenta et al., 2002; Lee et al., 2012). However, DPA is not registered for this use and the maximum residue limit (MRL) of 0.1 mg/kg imposed on apples by the European Commission is unachievable making its use impossible (Robatscher et al., 2012). In this study, fruit were exposed to a storage atmosphere with 0.1 % O_2 and 50 % CO_2 for 3 days after harvest at room temperature (21 °C) meaning that both low O_2 and high CO_2 acted as stress factors. The extremely low O_2 concentration may have aggravated the negative effect of high CO_2 in

Table 4
Three dimensional morphometric parameters of the pores of fruit tissue obtained from X-ray CT images of 'Fuji' apples after the high CO_2/low O_2 stress treatment. 3D indicates that the measurements were done on 3 dimensional structures.

	Surface area (μm^2)	Surface area/ volume ratio (μm^{-1})	Number of closed pores	Closed porosity (%)	Open porosity (%)	Total porosity (%)	Connectivity	Length3D (μm)	Sphericity	Anisotropy
Affected brown tissue	79.53 b	5.34 b	1666 ns	3.1 b	0.9 b	4.0 b	52.2 b	95.43 b	0.882 a	0.765 b
White tissue from affected fruit	176.96 a	12.80 a	2987	5.1 a	6.2 a	10.9 a	705.6 a	128.65 a	0.828 c	0.811 a
Unaffected tissue	188.37 a	13.69 a	3390	5.9 a	6.4 a	11.9 a	745.7 a	120.07 a	0.849 b	0.792 a
Pr > F(Model)	*< 0.0001*	*< 0.0001*	*0.121*	*< 0.0001*	*< 0.0001*	*< 0.0001*	*< 0.0001*	*0.002*	*0.000*	*0.001*
LSD value	*15.25*	*1.206*	*1433*	*0.881*	*1.604*	*1.933*	*101.609*	*15.337*	*0.02*	*0.02*

Results are indicated as mean values. Different letters for the same parameter indicate significant differences according to Fishers LSD at $p < 0.05$. ns represents non-significant differences.

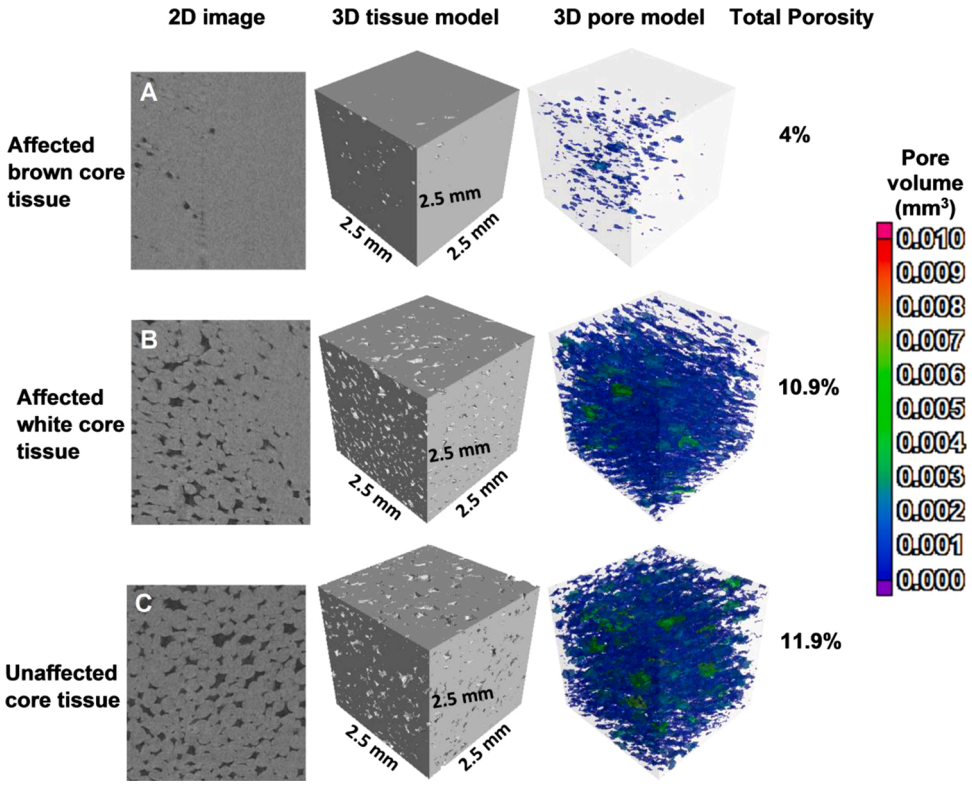

Fig. 5. 2D images after surface determination, 3D tissue models and 3D pore models of A - affected brown core tissue, B - white core tissue adjacent to affected brown tissue and C - unaffected core tissue of 'Fuji' apples after X-ray CT scanning and 3D image analysis of fruit tissue obtained from fruit after the high CO_2/low O_2 stress treatment. Pores are dark grey and fruit tissue is light grey. Different colours in the 3D pore models represent different pore volumes as shown in the scale.

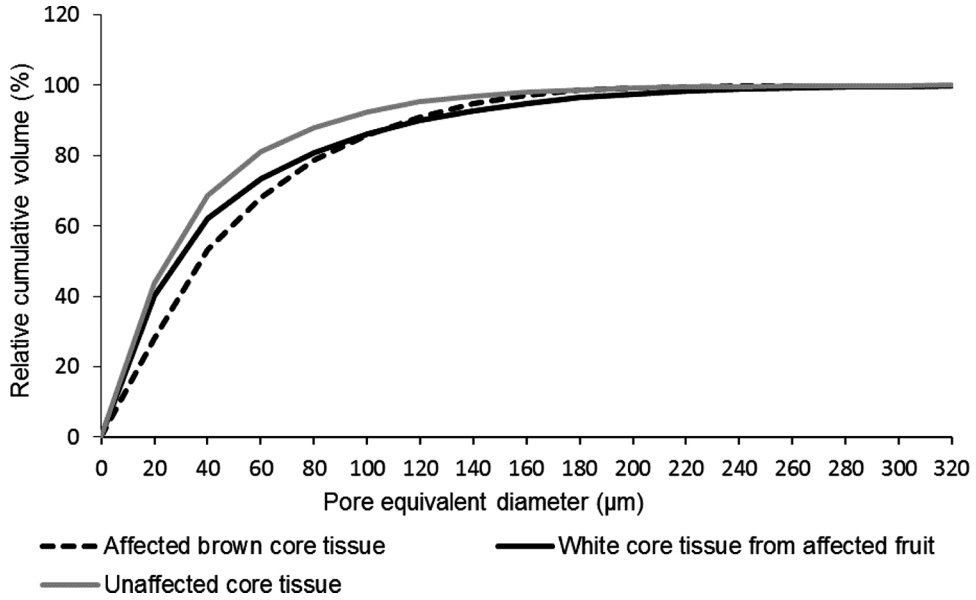

Fig. 6. Normal curve of distribution for individual pores in function of the equivalent diameter (µm) for affected brown core tissue, white core tissue from affected fruit and unaffected core tissue.

the storage atmosphere. In their studies on 'Bartlett' pear, Ke et al. (1994) found that a combination of high CO_2 and low O_2 in the storage atmosphere may induce ethanolic fermentation in fruit tissue due to increased amounts of pyruvate carboxylase (PDC) and alcohol dehydrogenase (ADH).

Short-term exposure of 'Fuji' apples to high CO_2 levels has been used as a reliable method to predict susceptibility of 'Fuji' apples to IB incidence during long-term storage (Argenta et al., 2002). The results of this study showed that there was incidence of IB to varying degrees after short-term exposure to high CO_2, however, all the browning occurred in the core region of the fruit (Fig. 7). The reason for the high incidence of IB in this region is unclear, but it might be due to the low porosity in the core region compared to the cortex region and the long radial distance of the core region from the fruit surface (Herremans et al., 2015). Nugraha

Table 5
Three dimensional morphometric parameters of the cells of fruit tissue obtained from X-ray CT images of 'Fuji' apples after the high CO_2/low O_2 stress treatment. 3D indicates that the measurements were done on 3 dimensional structures.

	Length3D (μm)	Thickness3D (μm)	Width3D (μm)	Area3D (mm^2)	Euler3D	Volume3D (mm^3)	Anisotropy	EqDiameter (μm)	Sphericity
Affected brown tissue	295.73 ns	167.61 ns	174.32 a	0.155 a	0.637 b	0.0035 ns	0.682 ns	178.82 ns	0.688 b
White tissue from affected fruit	285.92	157.75	160.86 b	0.139 b	0.902 a	0.0035	0.686	177.56	0.767 a
Unaffected tissue	287.24	159.88	162.74 b	0.139 b	0.921 a	0.0035	0.682	180.00	0.773 a
Pr > F(Model)	*0.277*	*0.062*	*0.004*	*0.002*	*< 0.0001*	*0.935*	*0.927*	*0.818*	*< 0.0001*
LSD value	*11.225*	*7.285*	*6.926*	*0.0086*	*0.039*	*0.0004*	*0.024*	*7.536*	*0.012*

Results are indicated as mean values. Different letters for the same parameter indicate significant differences according to Fisher's LSD at $p < 0.05$. ns represents non-significant difference.

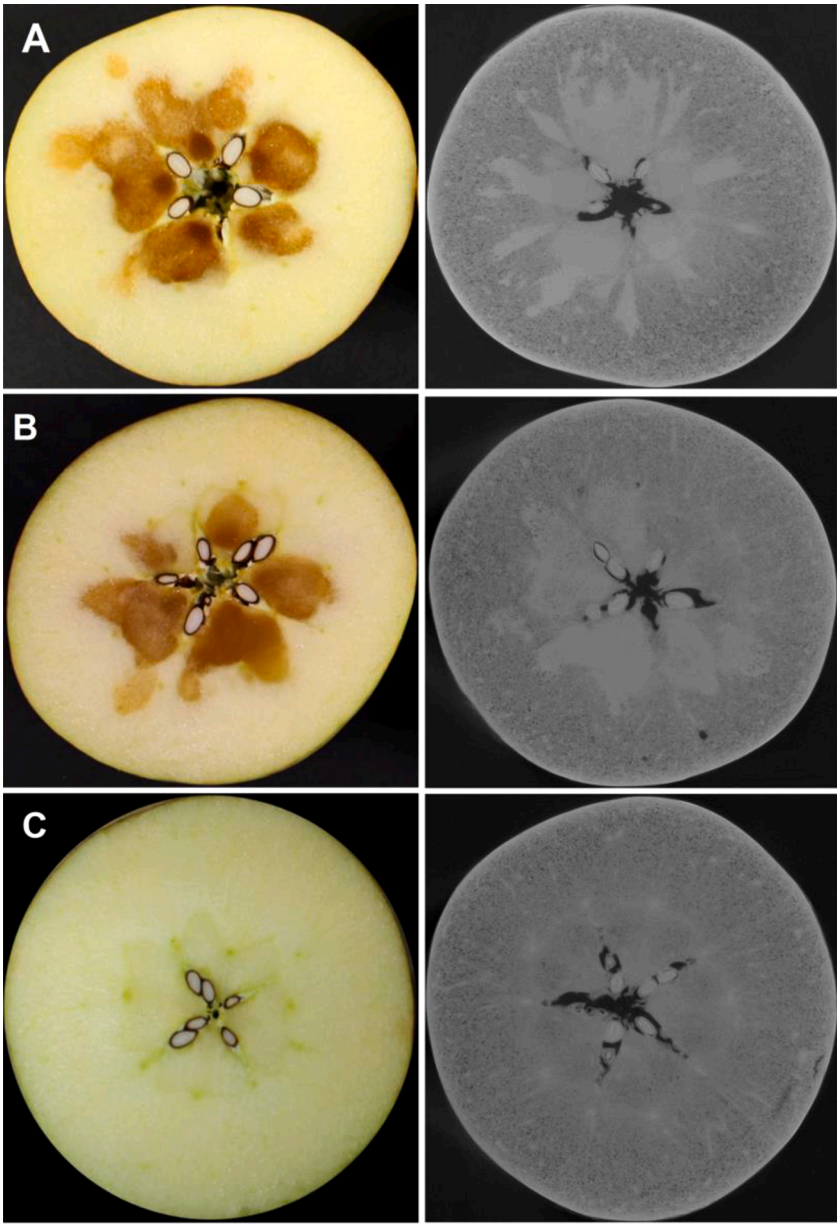

Fig. 7. Original images and corresponding greyscale images for A and B - fruit with IB in the core region and C - a fruit without IB in the core region. Low-resolution scans were done at a resolution of 60 μm on whole fruit after the high CO_2/low O_2 stress treatment.

et al. (2019) provided that the core region of 'Jonagold' apple fruit is made up of dense tissue with a porosity of 3–12 % while the cortex region is relatively more porous (12–35 %), in this study the porosity of healthy core region tissue was 10.9 %. Ting et al. (2013) reported a porosity of 29.3 % in the cortex of 'Fuji' apples. According to Herremans et al. (2013), the inner cortex of apples has low porosity and the pores are poorly connected, these microstructural properties hinder gaseous exchange in the core region of the fruit. The interaction of these factors

may cause insufficient movement of CO_2 in the core region leading to its accumulation and incidence of IB. However, CO_2 induced IB during long-term CA storage usually occurs in the cortex region and is sometimes accompanied by pits and cavities, susceptible cultivars include 'Braeburn', 'Kanzi', 'Elstar', 'Santana' and 'Fuji' (de Freitas and Pareek, 2019). IB observed in commercially stored South African 'Fuji' apples occurs in all regions of the fruit tissue and is not limited to only the core region.

While low porosity is a causative factor for IB incidence (Herremans et al., 2015), it is also an after-effect of IB occurring after short-term exposure to stress conditions since affected fruit tissue is characterised by reduced porosity (Chigwaya et al., 2018). This present study looked at the closed porosity, open porosity and total porosity, in all instances the porosity was significantly lower in brown affected tissue samples. The 3D pore models clearly showed the reduced porosity (4 %) in brown affected tissue samples (Fig. 5). This reduced porosity due to IB can be attributed to the damage of cells and membrane leakage leading to cellular fluids filling up the intercellular air spaces and rendering them ineffective to efficiently execute their role of respiratory gas transport (Herremans et al., 2013; Mellidou et al., 2014). During long-term cold storage, the cellular fluids and free water that floods the intercellular air spaces as a result of CO_2 induced membrane damage will diffuse out of the fruit as storage time progresses leaving large cavities in the affected tissue (Lau, 1998). However, this present study focused on the initial stages of CO_2 induced IB, which is characterised by flooding of the intercellular spaces with cellular fluids.

In addition to the reduced total porosity, affected brown tissue also had low pore connectivity. The poor connectivity of pores coupled with low porosity of affected tissue further aggravated the disorder (Schotsmans et al., 2004; Herremans et al., 2013). The connectivity looks at the connectedness of the pores and low pore connectivity indicates reduced capacity of the pores to efficiently transport respiratory gases (James and Jobling, 2009; Mebatsion et al., 2009; Verboven et al., 2013). In terms of size, the pores in brown affected tissue had a significantly smaller length and this shows that as the flooding of intercellular spaces progressed, the larger pores were eliminated first leaving behind smaller pores which are limited in their capacity to efficiently transport respiratory gases (Herremans et al., 2013). The sphericity of pores in affected brown tissue was significantly higher meaning that the pores in the affected tissue were more spherical than pores from unaffected tissue. The pores in apples fruit are normally randomly shaped with a less defined shape (Ting et al., 2013). The spherical shape of pores in affected tissue is a clear sign that the fruit microstructure was altered at a cellular level by IB. Low-resolution scans done on the fruit did not show significant differences in the tissue density of affected and unaffected tissue. However, differences in greyscale intensity were seen from the light grey colour of fruit tissue affected by IB as compared to the dark grey colour of tissue not affected by IB (Fig. 7). Pore anisotropy was low in brown affected tissue samples and this indicates loss of oriented structures as the browning progresses (Herremans et al., 2013).

The cellular structure of the fruit tissue was also affected by IB. The effect of IB on cellular structure has been highlighted by several (Argenta et al., 2000; de Castro et al., 2007, 2008). Normally, it is difficult to efficiently segment individual cells in X-ray CT images due to insufficient contrast between neighbouring cells, as a result, a watershed segmentation technique was utilised to isolate individual cells in this study (Ruparelia, 2012). When the watershed segmentation algorithm was applied to images from unaffected tissue samples, the cell-to-cell boundaries were clearly defined, however, this was not the case in images from tissue samples with IB. The cellular structure in brown affected tissue was severely disrupted to such an extent that neighbouring cells could not be distinguished from each other with the watershed separation method (Fig. 4). The failure of the watershed algorithm to detect the cell-to-cell boundaries shows that the cellular structure in brown samples was severely disrupted. As a result, only a few cells were properly isolated and obtainable for analysis. Cells from affected tissue had a smaller width and surface area compared to cells from unaffected tissue. The cells from affected tissue also had a significantly lower sphericity compared to cells from unaffected tissue, this can be attributed to cell damage due to loss of membrane integrity and membrane leakage (Saquet et al., 2000; Mellidou et al., 2014).

5. Conclusion

'Fuji' apples exposed to a storage atmosphere with 0.1 % O_2 and with 50 % CO_2 for 3 days after harvest at ambient temperature developed varying degrees of IB that was concentrated around the core region of the fruit. 3D image analysis showed that brown affected fruit tissue had significantly lower porosity and lower pore connectivity, due to filling of pore spaces with cellular fluids released after cell damage caused by the high CO_2/low O_2 stress. The sphericity of pores in brown affected tissue was significantly higher which points out to changes of fruit microstructure and changes in cellular structure as a result of IB development. Low porosity in specific regions of the fruit may play a role in predisposing fruit to localised development of CO_2 induced IB. Determination of microstructural parameters in relation to IB incidence will add value to the comprehensive understanding of postharvest handling and storage of 'Fuji' apples.

CRediT authorship contribution statement

Kenias Chigwaya: Conceptualization, Methodology, Investigation, Writing - original draft, Visualization, Project administration. **Anton du Plessis:** Methodology, Writing - review & editing. **Daniël W. Viljoen:** Methodology, Writing - review & editing. **Ian J. Crouch:** Methodology, Writing - review & editing. **Elke M. Crouch:** Conceptualization, Methodology, Writing - review & editing, Supervision, Project administration, Funding acquisition.

Declaration of Competing Interest

The authors declare that they have no known competing financial interests or personal relationships that could have appeared to influence the work reported in this paper.

Acknowledgements

The authors would like to thank the South African Apple and Pear Producer's Association and HORTGRO for funding this research. The authors also appreciate the travel grant awarded to Kenias Chigwaya to learn more about X-ray CT at the Division of Mechatronics, Biostatistics and Sensors (KU Leuven) by the Department of Horticultural Science and the Postgraduate office at Stellenbosch University. The technical support from the X-ray CT Scanner Facility at Stellenbosch University is appreciated.

References

Argenta, L., Fan, X., Mattheis, J., 2000. Delaying establishment of controlled atmosphere or CO_2 exposure reduces 'Fuji' apple CO_2 injury without excessive fruit quality loss. Postharvest Biol. Technol. 20, 221–229. https://doi.org/10.1016/S0925-5214(00)00134-4.

Argenta, L.C., Fan, X., Mattheis, J.P., 2002. Responses of 'Fuji' apples to short and long duration exposure to elevated CO_2 concentration. Postharvest Biol. Technol. 24, 13–24. https://doi.org/10.1016/S0925-5214(01)00120-X.

Argenta, L.C., do Amarante, C.V.T., Betinelli, K.S., Brancher, T.L., Nesi, C.N., Viera, M.J., 2020. Comparison of fruit attributes of 'Fuji' apple strains at harvest and after storage. Sci. Hortic. 272, 109585 https://doi.org/10.1016/j.scienta.2020.109585.

Boas, F.E., Fleischmann, D., 2012. CT artifacts: causes and reduction techniques. Imaging Med. 4, 229–240.

Chigwaya, K., Schoeman, L., Fourie, W.J., Crouch, I., Viljoen, D., Crouch, E.M., 2018. 'Fuji' apple internal browning explored via X-ray computed tomography (CT). Acta Hortic. 1201, 309–316. https://doi.org/10.17660/ActaHortic.2018.1201.42.

de Castro, E., Biasi, B., Mitcham, E., Tustin, S., Tanner, D., Jobling, J., 2007. Carbon dioxide-induced flesh browning in Pink Lady apples. Am. Soc. Hortic. 132, 713–719. https://doi.org/10.21273/JASHS.132.5.713.

de Castro, E., Barrett, D.M., Jobling, J., Mitcham, E.J., 2008. Biochemical factors associated with a CO_2-induced flesh browning disorder of Pink Lady apples. Postharvest Biol. Technol. 48, 182–191. https://doi.org/10.1016/j.postharvbio.2007.09.027.

de Freitas, S.T., Pareek, S. (Eds.), 2019. Postharvest Physiological Disorders in Fruits and Vegetables. CRC Press. https://doi.org/10.1201/b22001.

Diels, E., Dael, M. Van, Keresztes, J., Vanmaercke, S., Verboven, P., Nicolaï, B., Saeys, W., Ramon, H., Smeets, B., 2017. Assessment of bruise volumes in apples using X-ray computed tomography. Postharvest Biol. Technol. 128, 24–32. https://doi.org/10.1016/j.postharvbio.2017.01.013.

du Plessis, A., le Roux, S.G., Guelpa, A., 2016. The CT scanner facility at Stellenbosch University: an open access X-ray computed tomography laboratory. Nucl. Instruments Methods Phys. Res. Sect. B Beam Interact. Mater. Atoms 384, 42–49. https://doi.org/10.1016/j.nimb.2016.08.005.

du Plessis, A., Tshibalanganda, M., le Roux, S.G., 2020. Not all scans are equal: X-ray tomography image quality evaluation. Mater. Today Commun. 22, 100792 https://doi.org/10.1016/j.mtcomm.2019.100792.

Elgar, H.J., Lallu, N., Watkins, C.B., 1999. Harvest date and crop load effects on a carbon dioxide–related storage injury of `Braeburn' apple. HortScience 34, 305–309. https://doi.org/10.21273/hortsci.34.2.305.

Ferree, D.C., Warrington, I.J., 2003. Apples: Botany, Production and Uses. CABI. https://doi.org/10.1079/9780851995922.0000.

Guelpa, A., Plessis, A., Kidd, M., Manley, M., 2015. Non-destructive Estimation of Maize (*Zea mays* L.) Kernel Hardness by Means of an X-Ray Micro-Computed Tomography (μ CT) Density Calibration, pp. 1419–1429. https://doi.org/10.1007/s11947-015-1502-3.

Herremans, E., Verboven, P., Bongaers, E., Estrade, P., Verlinden, B.E., Wevers, M., Hertog, M.L.A.T.M., Nicolaï, B.M., 2013. Characterisation of 'Braeburn' browning disorder by means of X-ray micro-CT. Postharvest Biol. Technol. 75, 114–124. https://doi.org/10.1016/j.postharvbio.2012.08.008.

Herremans, E., Verboven, P., Verlinden, B.E., Cantre, D., Abera, M., Wevers, M., Nicolaï, B.M., 2015. Automatic analysis of the 3-D microstructure of fruit parenchyma tissue using X-ray micro-CT explains differences in aeration. BMC Plant Biol. 15, 1–14. https://doi.org/10.1186/s12870-015-0650-y.

Ho, Q.T., Verboven, P., Verlinden, B.E., Schenk, A., Nicolaï, B.M., 2013. Controlled atmosphere storage may lead to local ATP deficiency in apple. Postharvest Biol. Technol. 78, 103–112. https://doi.org/10.1016/j.postharvbio.2012.12.014.

HORTGRO, 2019. Key Deciduous Fruit Statistics. . Accessed 8 September 2020. https://www.hortgro.co.za/wp-content/uploads/docs/2020/07/key-deciduous-fruit-statistics-2019-1.pdf.

Iassonov, P., Gebrenegus, T., Tuller, M., 2009. Segmentation of X-ray computed tomography images of porous materials: a crucial step for characterization and quantitative analysis of pore structures. Water Resour. Res. 45, 1–12. https://doi.org/10.1029/2009WR008087.

James, H.J., Jobling, J.J., 2009. Contrasting the structure and morphology of the radial and diffuse flesh browning disorders and CO_2 injury of 'Cripps Pink' apples. Postharvest Biol. Technol. 53, 36–42. https://doi.org/10.1016/j.postharvbio.2009.02.001.

Ke, D., van Gorsel, H., Kader, A.A., 1990. Physiological and quality responses of `Bartlett' pears to reduced O_2 and enhanced CO_2 levels and storage temperature. J. Am. Soc. Hortic. Sci. 115, 435–439. https://doi.org/10.21273/jashs.115.3.435.

Ke, D., Yahia, E., Mateos, M., Kader, A.A., 1994. Ethanolic fermentation of 'Bartlett' pears as influenced by ripening stage and atmospheric composition. J. Am. Soc. Hortic. Sci. 119, 976–982. https://doi.org/10.21273/jashs.119.5.976.

Lau, O.L., 1998. Effect of growing season, harvest maturity, waxing, low O_2 and elevated CO_2 on flesh browning disorders in 'Braeburn' apples. Postharvest Biol. Technol. 14, 131–141. https://doi.org/10.1016/S0925-5214(98)00035-0.

Lee, J., Mattheis, J.P., Rudell, D.R., 2012. Antioxidant treatment alters metabolism associated with internal browning in 'Braeburn' apples during controlled atmosphere storage. Postharvest Biol. Technol. 68, 32–42. https://doi.org/10.1016/j.postharvbio.2012.01.009.

McAtee, P.A., Hallett, I.C., Johnston, J.W., Schaffer, R.J., 2009. A rapid method of fruit cell isolation for cell size and shape measurements. Plant Methods 5, 1–7. https://doi.org/10.1186/1746-4811-5-5.

Mebatsion, H.K., Verboven, P., Endalew, A.M., Billen, J., Ho, Q.T., Nicolaï, B.M., 2009. A novel method for 3-D microstructure modeling of pome fruit tissue using synchrotron radiation tomography images. J. Food Eng. 93, 141–148. https://doi.org/10.1016/j.jfoodeng.2009.01.008.

Mellidou, I., Buts, K., Hatoum, D., Ho, Q.T., Johnston, J.W., Watkins, C.B., Schaffer, R.J., Gapper, N.E., Giovannoni, J.J., Rudell, D.R., Hertog, M.L.A.T.M., Nicolaï, B.M., 2014. Transcriptomic events associated with internal browning of apple during postharvest storage. BMC Plant Biol. 14, 1–17. https://doi.org/10.1186/s12870-014-0328-x.

Mendoza, F., Verboven, P., Mebatsion, H.K., Kerckhofs, G., Wevers, M., Nicolaï, B., 2007. Three-dimensional pore space quantification of apple tissue using X-ray computed microtomography. Planta 226, 559–570. https://doi.org/10.1007/s00425-007-0504-4.

Muziri, T., Theron, K.I., Cantre, D., Wang, Z., Verboven, P., Nicolaï, B.M., Crouch, E.M., 2016. Microstructure analysis and detection of mealiness in 'Forelle' pear (*Pyrus communis L.*) by means of X-ray computed tomography. Postharvest Biol. Technol. 120, 145–156. https://doi.org/10.1016/j.postharvbio.2016.06.006.

Nugraha, B., Verboven, P., Janssen, S., Wang, Z., Nicolaï, B.M., 2019. Non-destructive porosity mapping of fruit and vegetables using X-ray CT. Postharvest Biol. Technol. 150, 80–88. https://doi.org/10.1016/j.postharvbio.2018.12.016.

Otsu, N., 1979. A threshold selection method from gray-level histograms. IEEE Trans. Syst. Man Cybern. 9, 62–66.

Pedreschi, R., Hertog, M., Robben, J., Noben, J.P., Nicolaï, B., 2008. Physiological implications of controlled atmosphere storage of 'Conference' pears (*Pyrus communis L.*): a proteomic approach. Postharvest Biol. Technol. 50, 110–116. https://doi.org/10.1016/j.postharvbio.2008.04.004.

Pedreschi, R., Franck, C., Lammertyn, J., Erban, A., Kopka, J., Hertog, M., Verlinden, B., Nicolaï, B., 2009a. Metabolic profiling of 'Conference' pears under low oxygen stress. Postharvest Biol. Technol. 51, 123–130. https://doi.org/10.1016/j.postharvbio.2008.05.019.

Pedreschi, R., Hertog, M., Robben, J., Lilley, K.S., Karp, N.A., Baggerman, G., Vanderleyden, J., Nicolaï, B., 2009b. Gel-based proteomics approach to the study of metabolic changes in pear tissue during storage. J. Agric. Food Chem. 57, 6997–7004. https://doi.org/10.1021/jf901432h.

Pieczywek, P.M., Zdunek, A., 2012. Automatic classification of cells and intercellular spaces of apple issue. Comput. Electron. Agric. 81, 72–78. https://doi.org/10.1016/j.compag.2011.11.006.

Poles, L., Gentile, A., Giuffrida, A., Valentini, L., Endrizzi, I., Aprea, E., Gasperi, F., Distefano, G., Artioli, G., La Malfa, S., Costa, F., Lovatti, L., Di Guardo, M., 2020. Role of fruit flesh cell morphology and MdPG1 allelotype in influencing juiciness and texture properties in apple. Postharvest Biol. Technol. 164 https://doi.org/10.1016/j.postharvbio.2020.111161.

Robatscher, P., Eisenstecken, D., Sacco, F., Pöhl, H., Berger, J., Zanella, A., Oberhuber, M., 2012. Diphenylamine residues in apples caused by contamination in fruit storage facilities. J. Agric. Food Chem. 60, 2205–2211. https://doi.org/10.1021/jf204477c.

Ruparelia, S., 2012. Implementation of Watershed Based Image Segmentation Algorithm in FPGA. Master's thesis. Department of Parallel Systems, University of Stuttgart, Stuttgart, Germany.

Saquet, A.A., Streif, J., Bangerth, F., 2000. Changes in ATP, ADP and pyridine nucleotide levels related to the incidence of physiological disorders in 'Conference' pears and 'Jonagold' apples during controlled atmosphere storage. J. Hortic. Sci. Biotechnol. 75, 243–249. https://doi.org/10.1080/14620316.2000.11511231.

Saquet, A.A., Streif, J., Bangerth, F., 2003. Energy metabolism and membrane lipid alterations in relation to brown heart development in 'Conference' pears during delayed controlled atmosphere storage. Postharvest Biol. Technol. 30, 123–132. https://doi.org/10.1016/S0925-5214(03)00099-1.

Schoeman, L., Williams, P., du Plessis, A., Manley, M., 2016. X-ray micro-computed tomography (μCT) for non-destructive characterisation of food microstructure. Trends Food Sci. Technol. https://doi.org/10.1016/j.tifs.2015.10.016.

Schotsmans, W., Verlinden, B.E., Lammertyn, J., Nicolaï, B.M., 2004. The relationship between gas transport properties and the histology of apple. J. Sci. Food Agric. 84, 1131–1140. https://doi.org/10.1002/jsfa.1768.

Tanaka, F., Tatsuki, M., Matsubara, K., Okazaki, K., Yoshimura, M., Kasai, S., 2018. Methyl ester generation associated with flesh browning in 'Fuji' apples after long storage under repressed ethylene function. Postharvest Biol. Technol. 145, 53–60. https://doi.org/10.1016/j.postharvbio.2018.06.002.

Ting, V.J.L., Silcock, P., Bremer, P.J., Biasioli, F., 2013. X-ray micro-computer tomographic method to visualize the microstructure of different apple cultivars. J. Food Sci. 78, E1735–E1742. https://doi.org/10.1111/1750-3841.12290.

Verboven, P., Herremans, E., Borisjuk, L., Helfen, L., Ho, Q.T., Tschiersch, H., Fuchs, J., Nicolaï, B.M., Rolletschek, H., 2013. Void space inside the developing seed of Brassica napus and the modelling of its function. New Phytol. 199, 936–947. https://doi.org/10.1111/nph.12342.

Vicent, V., Verboven, P., Ndoye, F.T., Alvarez, G., Nicolaï, B., 2017. A new method developed to characterize the 3D microstructure of frozen apple using X-ray micro-CT. J. Food Eng. 212, 154–164. https://doi.org/10.1016/j.jfoodeng.2017.05.028.

Wang, Z., Van Beers, R., Aernouts, B., Watté, R., Verboven, P., Nicolaï, B., Saeys, W., 2020. Microstructure affects light scattering in apples. Postharvest Biol. Technol. 159, 110996 https://doi.org/10.1016/j.postharvbio.2019.110996.

Zhang, P., Lu, S., Li, J., Zhang, P., Xie, L., Xue, H., Zhang, J., 2017. Multi-component segmentation of X-ray computed tomography (CT) image using multi-Otsu thresholding algorithm and scanning electron microscopy. Energy Explor. Exploit. 35, 281–294. https://doi.org/10.1177/0144598717690090.